

Unifying the Various Incarnations of Active Hair-Bundle Motility by the Vertebrate Hair Cell

Jean-Yves Tinevez,* Frank Jülicher,[†] and Pascal Martin*

*Laboratoire Physico-Chimie Curie, CNRS, Institut Curie, Paris, France; and [†]Max-Planck-Institute for the Physics of Complex Systems, Dresden, Germany

ABSTRACT The dazzling sensitivity and frequency selectivity of the vertebrate ear rely on mechanical amplification of the hair cells' responsiveness to small stimuli. As revealed by spontaneous oscillations and forms of mechanical excitability in response to force steps, the hair bundle that adorns each hair cell is both a mechanosensory antenna and a force generator that might participate in the amplificatory process. To study the various incarnations of active hair-bundle motility, we combined Ca^{2+} iontophoresis with mechanical stimulation of single hair bundles from the bullfrog's sacculus. We identified three classes of active hair-bundle movements: a hair bundle could be quiescent but display nonmonotonic twitches in response to either excitatory or inhibitory force steps, or oscillate spontaneously. Extracellular Ca^{2+} changes could affect the kinetics of motion and, when large enough, evoke transitions between the three classes of motility. We found that the Ca^{2+} -dependent location of a bundle's operating point within its force-displacement relation controlled the type of movement observed. In response to an iontophoretic pulse of Ca^{2+} or of a Ca^{2+} chelator, a hair bundle displayed a movement whose polarity could be reversed by applying a static bias to the bundle's position at rest. Moreover, such polarity reversal was accompanied by a 10-fold change in the kinetics of the Ca^{2+} -evoked hair-bundle movement. A unified theoretical description, in which mechanical activity stems solely from myosin-based adaptation, could account for the fast and slow manifestations of active hair-bundle motility observed in frog, as well as in auditory organs of the turtle and the rat.

INTRODUCTION

Sensory hair cells from the inner ear make use of mechanical amplification to respond most sensitively and selectively to faint stimuli (1). In the mammalian cochlea, the length of the outer hair cells is affected by changes in the membrane potential (2). This process of somatic electromotility has been proposed to play a key role in amplification (3). Recent evidence suggests that the cochlea also benefits from active motility of the mechanosensory hair bundle that adorns the apical surface of each hair cell (4,5). Nonmammalian hair cells lack somatic electromotility. In these cells, the motor that mediates amplification most probably resides in the hair bundle (6). Spontaneous hair-bundle oscillations (7–12) demonstrate that the hair bundle can drive hair-bundle deflections even in the absence of stimulation. It has been shown both experimentally (11,13) and theoretically (14–16) that the hair cell can mobilize these active movements to enhance its sensitivity and frequency selectivity to minute stimuli.

Hair bundles that do not oscillate spontaneously can also show signatures of mechanical activity, most often when stimulated by positive step forces that tend to open transduction channels (8,17,18). Within an appropriate range

of stimulus magnitudes, the hair-bundle produces a non-monotonic response called “twitch”: the motion in the direction of the applied force is interrupted by a fast recoil. This movement in opposition to the external force is associated on a similar timescale with reclosure of the transduction channels, a process often called fast adaptation. A second component of adaptation has been distinguished in the transduction current by a relaxation time that is one or more orders of magnitude longer than that characteristic of fast adaptation (19,20). Slow adaptation is correlated with a hair-bundle movement of similar time course but of directionality opposite that of the recoil seen in twitches (8,17). To interpret these observations, it has been proposed that two separate mechanisms of force production are at work in a hair bundle, each prompted by the calcium component of the transduction current but with conflicting effects on hair-bundle movements (17,21–23): in addition to the forces produced by a myosin-based adaptation motor, calcium might interact with some component of the transduction apparatus to favor the closed conformation of the transduction channels. Here, we show that adaptive movements of the myosin-based motor suffice to account for fast and slow hair-bundle movements of opposite directionality as well as for spontaneous oscillations.

MATERIALS AND METHODS

Experimental preparation

Each experiment was performed at a room temperature of 21–24°C with hair cells from the saccule of an adult bullfrog (*Rana catesbeiana*). During the

Submitted March 9, 2007, and accepted for publication June 29, 2007.

Address reprint requests to Dr. P. Martin, Laboratoire Physico-Chimie Curie, Institut Curie recherche, 26 rue d'Ulm, 75248 Paris cedex 05, France. Tel.: 33-1-42-34-67-48; Fax: 33-1-40-51-06-36; E-mail: pascal.martin@curie.fr.

Jean-Yves Tinevez's present address is Max-Planck Institute of Molecular Cell Biology and Genetics, Pfötenhauerstrasse 108, 01307 Dresden, Germany.

Editor: Robert Hsiu-Ping Chow.

© 2007 by the Biophysical Society
0006-3495/07/12/4053/15 \$2.00

doi: 10.1529/biophysj.107.108498

dissection, the sensory epithelium was totally immersed in oxygenated standard saline containing 110 mM Na⁺, 2 mM K⁺, 4 mM Ca²⁺, 122 mM Cl⁻, 3 mM D-glucose, 2 mM creatine phosphate, 2 mM sodium pyruvate, and 5 mM HEPES. The saccular macula was glued over a ~1-mm hole in a plastic film with tissue-compatible acrylic adhesive (Iso-dent, Ellman International, Hewlett, NY). The preparation was mounted on a two-compartment chamber to expose its apical and basal aspects to different ionic fluids and thereby mimic the native physiological conditions (11). While the basolateral surface was bathed by standard saline, hair bundles projected in NMDG artificial endolymph containing 2 mM Na⁺, 3 mM K⁺, 0.25 mM Ca²⁺, 110 mM N-methyl-D-glucamine, 111 mM Cl⁻, 3 mM D-glucose, and 5 mM HEPES. After exposing the apical surface of the hair cells for 25 min to endolymph that had been supplemented with the protease subtilisin (type XXIV; Sigma, St. Louis, MO) at a concentration of 50–67 μg ml⁻¹, the otolithic membrane was peeled off the macula to get access to individual hair bundles. Each solution had a pH of ~7.3 and an osmotic strength of ~230 mmol kg⁻¹.

Microscopic apparatus

The experimental chamber was secured to the rotary stage (U-SRG-2, Olympus, Tokyo, Japan) of an upright microscope (BX51WI, Olympus). The preparation was viewed using bright-field illumination through a ×60 water-immersion objective lens of 0.9 numerical aperture, a ×1.25 relay lens, and a dual camera port (WI-DPMC, Olympus). This dual port allowed simultaneous observation of the preparation with a camera (LCL-902K, Watec, Orangeburg, NY) and measurement of hair-bundle movements with a displacement monitor. This monitor included a dual photodiode (PIN-SPOT2D, UDT Sensor, Hawthorne, CA) onto which the tip of a hair bundle, or of a stimulus fiber attached to it, was imaged at a magnification of ×1000. A pair of preamplifiers directly attached to the photodiodes provided current-to-voltage conversion with a gain of 10⁷. The resulting voltages were subtracted and further amplified with an adjustable gain of 5–20 (AMP502, Tektronics, Beaverton, OR) to yield an output linearly proportional to the displacement of the fiber in a range of ±500 nm with a resolution of ~1 μm, corresponding to a ~1 nm resolution at the specimen plane. This photometric system was characterized by a bandwidth of 6.5 kHz at half the maximal power. The dual photodiode and attached circuitry were mounted on a piezoelectric stimulator that allowed calibration of each experimental record by measuring the output voltages of the photometric system in response to a series of offset displacements.

Mechanical stimulation

Hair bundles were stimulated with flexible glass fibers that were fabricated from borosilicate capillaries of 1.2-mm diameter (TW120-3, World Precision Instrument, Sarasota, FL) by published methods (12). To enhance optical contrast, the fibers were coated with a ~100-nm layer of gold-palladium (Hummer 6.2, Anatech, Hayward, CA). The stiffness K_F and drag coefficient λ_F of the fibers were, respectively, 150–500 μN m⁻¹ and 40–200 nN s m⁻¹, as determined by power spectral analysis of Brownian motion of the fiber's tip in water. Each fiber behaved as a first-order low-pass filter with a cutoff frequency of 430–2200 Hz.

The fiber was secured by its base to a stack-type piezoelectric actuator (PA 8/14, Piezosystem Jena, Hopedale, MA) driven by a low-noise power supply (ENV 150 and ENT 150/20, Piezosystem Jena). When powered by an unfiltered, abrupt voltage step, the actuator with an attached rigid fiber displayed a mechanical resonance at ~4 kHz. The actuator was in turn mounted on a Huxley micromanipulator (MP-85, Sutter Instrument, Novato, CA) that allowed fine positioning of the fiber's tip with submicrometer resolution.

The fiber's tip was affixed to the kinociliary bulb of an individual hair bundle, at a position situated 6.7 μm above the apical surface of the hair cell (24). Freshly made fibers adhered naturally. Neglecting viscous components,

the force F exerted by the stimulus fiber at the bundle's top was proportional to the deflection of the fiber. A movement Δ of the fiber's base elicited a force $K_F(\Delta - \bar{X})$, in which \bar{X} is the hair-bundle deflection evoked by this force. The hair bundle of interest was oriented to align the stimulation axis with that of maximal mechanosensitivity.

By using a flexible glass fiber and displacement-clamp circuitry (12,25), an oscillating hair bundle could be brought to a stable position X^S , at which, by convention, the external force F was set to zero. To characterize a bundle's mechanical properties, we applied a series of step displacements with respect to the steady-state position and measured the forces that had to be exerted to hold the hair bundle at these positions. For each displacement step, we estimated the elastic response of the hair bundle by recording the force ~3 ms after the onset of stimulation to allow just enough time for the viscous response to vanish and minimize the mechanical relaxation provided by adaptation (25). In accordance with the gating-spring model of mechano-electrical transduction (21,25), we fit the resulting force-displacement relation with

$$F = K_\infty \bar{X} - NZP_o + F_o, \quad (1)$$

in which K_∞ is the hair-bundle stiffness for large positive or negative displacements, N is the number of transduction elements, Z is the gating force associated with opening of a single transduction channel, and F_o is a constant force (Table 1). The probability P_o for a transduction channel to be open obeys the relation

$$P_o = \frac{1}{1 + \exp\left(\frac{Z(\bar{X} - \bar{X}_0)}{k_B T}\right)}, \quad (2)$$

in which \bar{X}_0 is the hair-bundle deflection at which $P_o = 0.5$.

Signal generation and collection

Stimulation and recordings were performed under the control of a computer running LabVIEW software (version 7.0; National Instruments, Austin, TX). Stimulus and calibration commands were generated by a dedicated interface (PCI-6713; National Instruments). Analog signals were low-pass filtered with an eight-pole Bessel filter adjusted to a half-power frequency of 1 kHz and then converted into digital signals at a sampling rate of 2.5 kHz and a precision of 12 bits using an interface card (PCI-MIO-16E1; National Instruments).

Iontophoresis of Ca²⁺ and Ca²⁺ chelators

We used iontophoresis to study the effects of Ca²⁺ on active hair-bundle motility and on the underlying force-displacement relations. Coarse microelectrodes were fabricated from borosilicate capillaries with a pipette puller (P97, Sutter Instrument), bent through an angle of ~90° in their tapered region and then filled either with 2.5 M CaCl₂, 350 mM disodium ATP, or 400 mM pentasodium triphosphate. We employed here ATP to chelate Ca²⁺ ions (12,26). Although ATP has been shown to gate purinergic receptors in the hair bundles of mammalian outer hair cells (27,28), there is no indication that similar receptors are present in hair bundles from the bullfrog's sacculus (29). If that were the case, ATP would be expected to increase, not decrease, the intracellular Ca²⁺ concentration. Consistent with the assumption that the main effect of ATP is here to chelate Ca²⁺, triphosphate had similar effects on the mechanical properties of a hair bundle as those attributed to ATP. When an electrode filled with CaCl₂ was immersed in NMDG-endolymph, its resistance ranged from 5 to 50 MΩ. In each experiment, the electrode's tip was situated within the horizontal plane of stimulation to ~3 μm from a hair bundle along an axis perpendicular to that of mechanical stimulation. To counteract the diffusive release of ions from the electrode, a holding current was applied under control conditions (12). In the case of Ca²⁺ iontophoresis, the transference number $\zeta \approx 12\%$ of

TABLE 1 Variables definition

Variable	Definition	
F	External force applied to the hair bundle's top	
K_F	Stiffness of stimulus fiber	
γ	Geometrical gain for a given hair bundle	
X	Position of the hair bundle's top with respect to the position that the bundle would assume if the gating springs were cleaved	
X^s	Position of the hair bundle at steady state for $F = 0$	
\bar{X}	Deflection of the hair bundle	$\bar{X} = X - X^s$
K_{GS}	Apparent combined stiffness of the gating springs for displacements along the axis of mechanical stimulation	
k_{GS}	Stiffness of a single gating spring along the axis of stereociliary shear	$K_{GS}/N\gamma^2$
K_{SP}	Apparent combined stiffness of the stereociliary pivots and the stimulus fiber for displacements along the axis of mechanical stimulation	
K_∞	Hair-bundle stiffness for large positive or negative displacements	$K_\infty = K_{GS} + K_{SP}$
D	Hair-bundle deflection that compensates the decrease in gating-spring extension that results from the opening of a transduction channel	
d	Microscopic gating swing; reduction of gating-spring extension on channel opening	$d = \gamma D$
N	Number of transduction elements	
Z	Gating force associated with the opening of a single transduction channel	$Z = K_{GS}D/N$
P_o	Open probability of the transduction channels	
A	The channels' open probability when the gating springs are severed is $1/(1 + A)$	
$k_B T$	Thermal energy where k_B is the Boltzmann constant and T is the temperature	
δ	Characteristic length of mechanosensitivity	$\delta = k_B T/Z$
X_a	Position of the adaptation motor with respect to the position for which the gating springs bear no tension if $X = 0$ and $P_o = 0$	
X_a^s	Motor position at steady state	
\bar{X}_a	Motor movement with respect to steady-state position	$\bar{X}_a = X_a - X_a^s$
\bar{X}_o	Deflection of the hair bundle for which $P_o = 0.5$	$\bar{X}_o = X_a - X^s + \frac{k_B T}{Z} \ln(A)$
K_{ES}	Apparent combined stiffness of the extent springs	
X_{ES}	Motor position at which the extent springs bear no tension	
λ	Friction coefficient of the hair bundle and attached stimulus fiber	
λ_a	Slope of the force-velocity relation of the adaptation motor	
F_a	Force that the adaptation motor produces at stall	
F_{max}	Stall force when $P_o = 0$	
$[Ca^{2+}]_0$	Ca^{2+} concentration at motor site with $P_o = 0$	
$[Ca^{2+}]_M$	Ca^{2+} concentration at motor site with $P_o = 1$	$[Ca^{2+}]_0 \ll [Ca^{2+}]_M$
S	Strength of the Ca^{2+} feedback on the motor force	$S = \frac{-[Ca^{2+}]_M}{F_{max}} \left. \frac{dF_a}{d[Ca^{2+}]} \right _{REF}$
v_{max}	Maximal velocity of the adaptation motor, along its axis of motion, if it were subjected to no load and if its force-velocity relation were linear	$v_{max} = \gamma F_{max}/\lambda_a$

All displacements and forces are expressed along the horizontal axis of a bundle's vertical plane of bilateral symmetry that contains the point of application of the external force.

Ca^{2+} ions was determined by a fluorimetric method. At a distance $r = 3 \mu m$ from the hair bundle, this technique allowed an increase of $\sim 20 \mu M$ of Ca^{2+} concentration per nanoampere of iontophoretic current.

Theoretical description of active hair-bundle mechanics

Variables definition is recapitulated in Table 1. The dynamic interplay between the positions X of the hair bundle and X_a of the adaptation motor is described by two coupled equations (12,30):

$$\lambda \frac{dX}{dt} = -K_{GS}(X - X_a - DP_o) - K_{SP}X + F + \eta \quad (3)$$

$$\lambda_a \frac{dX_a}{dt} = K_{GS}(X - X_a - DP_o) - K_{ES}(X_a - X_{ES}) - F_a + \eta_a. \quad (4)$$

The external force F is applied at the hair bundle's top along the horizontal axis of a hair bundle's vertical plane of bilateral symmetry. All variables are here expressed along this axis. In the absence of gating springs, the hair bundle is at position $X = 0$. The displacements of the adaptation motor are measured with respect to a position $X_a = 0$ for which the gating springs bear no tension if $X = 0$ and the channels are all closed. We assume that N identical transduction elements, each comprising a gating spring attached to a single transduction channel operate in parallel (21,24,31,32). The open probability P_o of the transduction channels is a nonlinear function of the relative position between the hair bundle and the adaptation motor:

$$P_o = \frac{1}{1 + A \exp\left(\frac{Z(X - X_a)}{k_B T}\right)}. \quad (5)$$

Here, $1/(1 + A)$ is the open probability of the transduction channels when the gating springs are severed and $Z = K_{GS}D/N$ is the gating force of a single transduction element. Identifying Eq. 5 with Eq. 2 yields

$$\bar{X}_0 = X_a - X^S + \frac{k_B T}{Z} \ln(A), \quad (6)$$

for the deflection \bar{X}_0 at which half of the transduction channels are open, in which X^S is the bundle's steady-state position when no external force is applied.

Equation 3 describes the dynamical behavior of the hair-bundle position X in response to the external force F . The hair bundle moves at a velocity that is inversely proportional to the friction coefficient λ . At steady-state ($dX/dt = 0$), F is balanced by the sum of the elastic restoring force $K_{SP}X$ provided by the stereociliary pivots and the total tension $T_{GS} = K_{GS}(X - X_a - DP_0)$ in the gating springs. Here, K_{GS} and K_{SP} correspond to the stiffness of the gating springs and of the stereociliary pivots, respectively. Channel opening decreases gating-spring extension by a distance that amounts to a horizontal displacement D at the bundle's top (21). Passive hair-bundle mechanics is characterized by the intrinsic force-displacement relation (Eq. 1). This relation describes the external force F as a function of the hair-bundle deflection $\bar{X} = X - X^S$ with the adaptation motor fixed at its steady-state position for $F = 0$. If relaxation of the bundle position X is much faster than that of the motor position X_a , one can estimate the intrinsic force-displacement relation by applying step displacements to the hair bundle and measuring force and displacement immediately after the hair-bundle position has reached steady state. The noise term η accounts for fluctuations that arise from the Brownian motion of fluid molecules and the stochastic gating of transduction channels (30).

Active hair-bundle movements result from the force produced by the adaptation motor (33). Equation 4 describes the dynamical behavior of this motor by a force-velocity relation of slope λ_a . Assuming that the motor operates near stall force F_a , we restrict a general expansion to linear order in $F_{\text{mot}} - F_a$, in which the external force that the motor experiences $F_{\text{mot}} = T_{GS} + T_{ES}$ is the combined tensions of the gating springs T_{GS} and of extent springs $T_{ES} = -K_{ES}(X_a - X_{ES})$. Here, X_{ES} is the value of X_a for which the extent springs bear no tension and K_{ES} is the combined stiffness of the extent springs. The extent springs anchor the transduction apparatus to the stereociliary cytoskeleton and account for the incompleteness of adaptation (34). At stall, F_a is balanced by F_{mot} . Active force production by the motors corresponds to motors climbing up the actin core of the stereocilia, i.e., $dX_a/dt < 0$, which tends to increase the extension of the gating springs and thus open the transduction channels. The stochastic activity of the molecular motors generates a stochastic force η_a (30,35).

To account for the regulation of adaptation by Ca^{2+} (36,37), we assume that the stall force produced by the motors depends instantaneously on the Ca^{2+} concentration $[\text{Ca}^{2+}]$ at the motor site

$$F_a \cong F_{\text{max}} + \frac{dF_a}{d[\text{Ca}^{2+}]} \Big|_{\text{REF}} [\text{Ca}^{2+}], \quad (7)$$

in which F_{max} is the maximal stall force that the motors can generate. Equation 7 represents the truncation to linear order of a general expansion of F_a in powers of $[\text{Ca}^{2+}]$ at a reference Ca^{2+} concentration. Imposing $(dF_a/d[\text{Ca}^{2+}])|_{\text{REF}} < 0$ ensures that increased Ca^{2+} levels at the motor site reduce active force generation and thus result in lower open probabilities of the transduction channels (36,38). Assuming that relaxation of the Ca^{2+} concentration occurs on a shorter timescale than hair-bundle movements, the Ca^{2+} concentration at the motor site is approximately determined by the open probability of the transduction channels:

$$[\text{Ca}^{2+}] \cong [\text{Ca}^{2+}]_0 + [\text{Ca}^{2+}]_M P_o. \quad (8)$$

Here, $[\text{Ca}^{2+}]_0$ and $[\text{Ca}^{2+}]_M$ denote the steady-state Ca^{2+} concentration when all channels are closed and the maximal Ca^{2+} concentration at the motor site when all channels are open, respectively; we note that $[\text{Ca}^{2+}]_M \gg [\text{Ca}^{2+}]_0$. By combining Eqs. 7 and 8, we find:

$$F_a \cong F_{\text{max}}(1 - S P_o), \quad (9)$$

in which the dimensionless parameter

$$S = - \frac{[\text{Ca}^{2+}]_M}{F_{\text{max}}} \frac{dF_a}{d[\text{Ca}^{2+}]} \Big|_{\text{REF}}, \quad (10)$$

defines the strength of the Ca^{2+} feedback on the motor force.

Parameter S is crucial, for it embodies electromechanical feedback of the Ca^{2+} component of the transduction current on the force that the adaptation motor can produce. We assume that the motor's activity is regulated by Ca^{2+} ions that freely diffuse from the channels' pores into the stereociliary cytoplasm (39). The maximal Ca^{2+} concentration at the motor site can then be estimated as a function of the extracellular Ca^{2+} concentration $[\text{Ca}^{2+}]_{\text{EXT}}$ at the channel's pore

$$[\text{Ca}^{2+}]_M \cong \alpha [\text{Ca}^{2+}]_{\text{EXT}}. \quad (11)$$

Numerically, $\alpha \approx 4\%$ if the Ca^{2+} sensor of the adaptation motor is located 20 nm from the channel's pore (12). Under these assumptions, the Ca^{2+} -feedback strength S varies linearly with the extracellular Ca^{2+} concentration, which can be modulated experimentally by Ca^{2+} iontophoresis. The steady-state concentration achieved at a distance r from the tip of an iontophoretic electrode can be estimated by assuming that Ca^{2+} ions simply diffused in a three-dimensional infinite volume (40)

$$[\text{Ca}^{2+}]_{\text{EXT}} = C_0 + \frac{\zeta I}{4\pi D_{\text{Ca}} z_{\text{Ca}} F_{\text{rd}} r}, \quad (12)$$

in which C_0 is the calcium concentration when no current is applied, ζ is the fraction of the total iontophoretic current I carried by calcium, $D_{\text{Ca}} = 800 \mu\text{m}^2 \text{s}^{-1}$ the diffusion coefficient of calcium in water, $z_{\text{Ca}} = 2$ the valence of calcium, and F_{rd} is the Faraday constant. By combining Eqs. 10, 11, and 12, one finds

$$S = S_0 + \frac{\beta}{F_{\text{max}}} \frac{dF_a}{d[\text{Ca}^{2+}]} \Big|_{\text{REF}} I, \quad (13)$$

in which S_0 is the value of S for an iontophoretic current $I = 0$ and $\beta = [\text{Ca}^{2+}]_M I$ is a constant that depends on the distance of the iontophoretic pipette to the hair bundle:

$$\beta = \frac{\alpha \zeta}{4\pi D_{\text{Ca}} z_{\text{Ca}} F_{\text{rd}} r}. \quad (14)$$

Simulations

We performed both deterministic and stochastic simulations. In deterministic simulations, $\eta = \eta_a = 0$. For a given set of parameter values and with $\Delta = 0$, we determined the stationary states $X = X^*$ and $X_a = X_a^*$ by solving Eqs. 3 and 4 with $dX/dt = dX_a/dt = 0$. In general, the system yields either one or three stationary states, but for the parameters considered here only one stationary state exists. Starting from this stationary state and using a Runge-Kunta algorithm (ODE45) in Matlab, version 7.0 (The MathWorks, Natick, MA), we numerically solve Eqs. 3 and 4 in cases where the fiber's base displacement Δ or the Ca^{2+} -feedback strength S vary as a function of time. To mimic experimental circumstances, we considered step stimuli. The response of the combined system of a hair bundle and its attached stimulus fiber of stiffness K_F to a movement Δ of the fiber's base was computed by setting $F = K_F \Delta$. For numerical calculations, parameter K_{SP} in turn corresponded to the summed stiffness of the stereociliary pivots and fiber and the friction coefficient λ includes that of the fiber and of the hair bundle (Table 1). Stochastic simulations were also performed to account for the effects of fluctuations as described previously (30).

RESULTS

Classification of active hair-bundle movements

We identified three classes of active hair-bundle movements (Fig. 1). First, a quiescent hair bundle could display a complex,

nonmonotonic twitch (18) in response to positively directed mechanical stimuli but not to stimuli of opposite directionality (Fig. 1 A). The initial movement in the direction of the applied force was interrupted within the first few milliseconds by a recoil, before the bundle slowly relaxed back in the direction of the stimulus toward a steady-state position. The twitch was associated with a nonlinear region of small slope in the force-displacement relation that was centered at a positive position with respect to the operating point of the hair bundle. Second, a hair bundle could oscillate spontaneously (Fig. 1 B). Each half-cycle of an oscillation was composed of a fast stroke in one direction followed by a slow movement in the same direction (12). As recognized before (25), the force-displacement relation of an oscillatory hair bundle typically displayed a region of negative slope that included the bundle's operating point. Third, we also observed quiescent hair bundles that displayed twitches, but only in response to negatively directed stimuli (Fig. 1 C). Twitches evoked by negative stimulation differed from those elicited by positive stimulation by their slower kinetics. The two types of twitches were also associated with force-displacement relations that were centered at displacements of opposite signs with respect to the operation point (compare Fig. 1, A and C).

To interpret these observations, we used a simple physical description of hair-bundle mechanics that is based on only three components: a force-displacement relation that contains a nonlinear region of reduced slope as the result of gating

compliance, adaptation motors that exert an active force against elastic gating springs, and electromechanical feedback by the calcium component of the transduction current on the force that the adaptation motor can produce at stall (see Materials and Methods). Numerically solving the dynamic Eqs. 3 and 4 for the position X of the hair bundle and X_a of the adaptation motor (Table 1), together with Eq. 9 that describes Ca^{2+} feedback on the motor's activity, we could mimic the three classes of active hair-bundle movements that we have observed in the bullfrog (Fig. 2). In each case, we adjusted the parameters to impose force-displacement relations that resembled those we measured and ensure that the system's operating point was adequately positioned. With a force-displacement relation that displayed a compliant region centered at a positive displacement with respect to the operating point, our simulations produced fast twitches in response to positive step forces (Fig. 2 A) but not with forces of opposite directionality (not shown). In this case, although the calculated movement of the hair bundle showed a recoil, the position X_a of the adaptation motor displayed a monotonic relaxation toward a new steady-state position. This behavior can be explained as follows. From Eq. 3 it follows that a small movement of the adaptation motor δX_a evokes a hair-bundle displacement δX that satisfies

$$\delta X \approx \frac{\bar{K}_{GS}}{\bar{K}_{GS} + K_{SP}} \delta X_a, \quad (15)$$

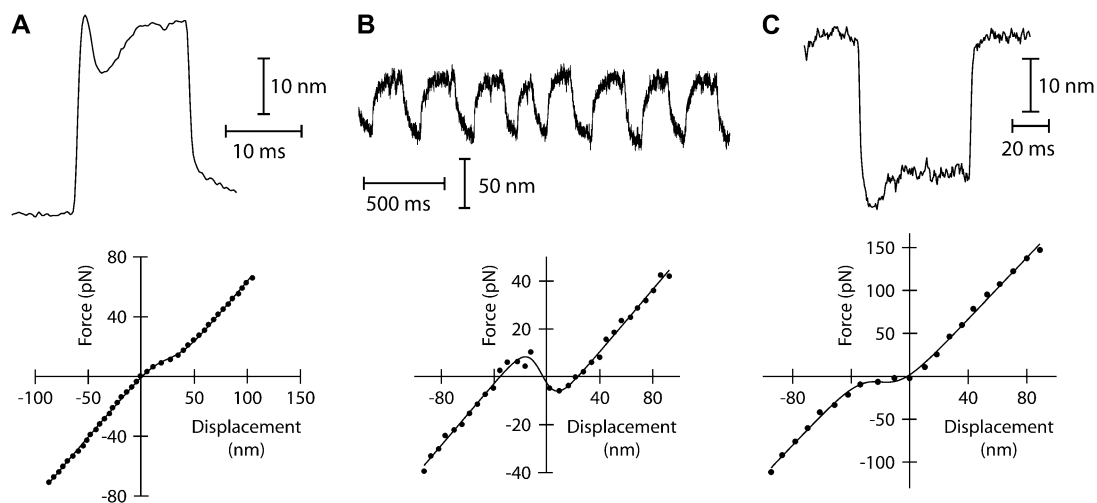


FIGURE 1 Three classes of active hair-bundle movements and associated force-displacement relations. (A) Positive twitch (average of 20 presentations). This quiescent hair bundle was stimulated by applying a step displacement of +137 nm to the base of the stimulus fiber. The initial movement in the direction of the stimulus was interrupted by a recoil of 5.6-ms duration and of 10-nm magnitude. After reaching a local minimum, the hair bundle relaxed toward a steady state in the positive direction. The force-displacement relation of the same hair bundle displayed a compliant region that was centered at +25 nm with respect to the origin of the graph. A fit of this curve with Eq. 1 (continuous line) yielded $K_{\infty} = 830 \mu\text{N m}^{-1}$, $N = 50$, and $Z = 0.41$ pN. The sensory epithelium was here immersed in standard saline with 4 mM Ca^{2+} . The fiber had a stiffness of $K_F = 270 \mu\text{N m}^{-1}$. (B) Spontaneous oscillations. This hair bundle showed spontaneous oscillations at a frequency of ~ 12 Hz and with a round-mean-squared (RMS) magnitude of 22 nm. Its force-displacement relation displayed a region of negative slope that included the origin of the graph. A fit of this curve with Eq. 1 gave $K_{\infty} = 650 \mu\text{N m}^{-1}$, $N = 56$, and $Z = 0.68$ pN. The artificial endolymph contained 250 μM Ca^{2+} . (C) Negative twitch (average of five presentations). In response to a -60 -nm step displacement of the stimulus fiber's base, this hair bundle displayed a recoil that lasted 29 ms with a magnitude of 7 nm. No recoil was observed in response to positively directed stimuli. The fiber had a stiffness of $K_F = 739 \mu\text{N m}^{-1}$. The force-displacement curve displayed a flat region that was centered at -21 nm with respect to the origin of the graph. A fit with Eq. 1 yielded $K_{\infty} = 1.8 \text{ mN m}^{-1}$, $N = 165$, and $Z = 0.44$ pN. The artificial endolymph contained 250 μM Ca^{2+} .

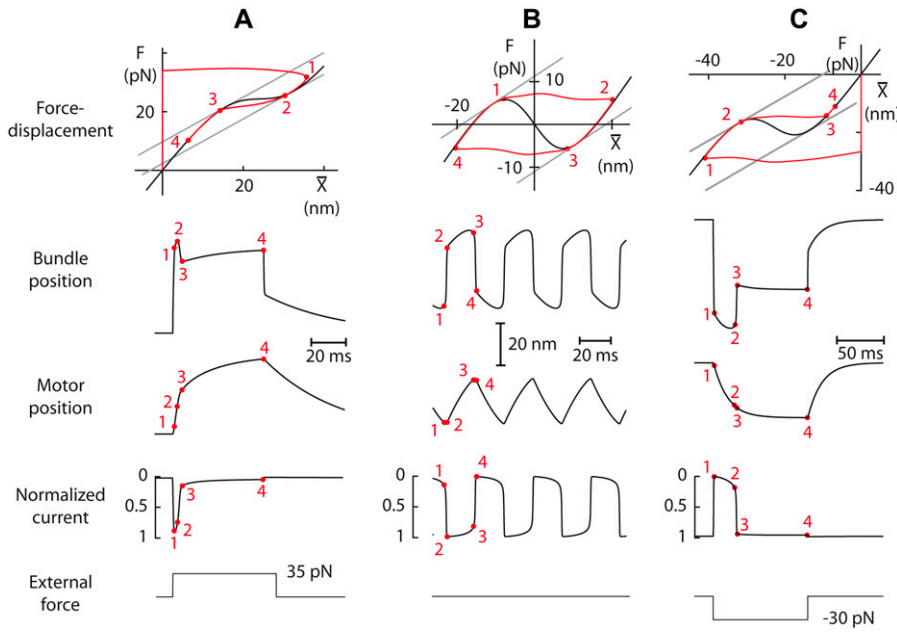


FIGURE 2 Simulations of active hair-bundle movements. In each case, the top figure (*black line*) describes the intrinsic force-displacement relation of a hair bundle attached to a stimulus fiber. The origin of the graph defines the system's operating point. When subjected to the force F whose time course is shown at the bottom, the positions of the hair bundle \bar{X} and of the adaptation motor \bar{X}_a as well as the normalized transduction current $-P_o$ vary with time. The trajectory superimposed in red on the force-displacement relation represents the force $F - K_{SP}\bar{X}_a$ as a function of the relative position $\bar{X} - \bar{X}_a$, where K_{SP} is the combined stiffness of the stereociliary pivots and of the stimulus fiber (Table 1). (A) Positive twitch. We imposed a force-displacement relation that was everywhere of positive slope but displayed a compliant nonlinear region delimited by two oblique straight lines (*gray*) of slope K_{SP} . This region was centered at a position of +18 nm with respect to the operating point. The brisk application of a +35 pN force first evoked a fast positive movement of the hair bundle that opened most of the transduction

channels, whereas the adaptation motor remained near its steady-state position (point 1). The motor then started to react to the sustained stimulus, by promoting an adaptive bundle movement in the positive direction and the reclosure of 9% of the transduction channels (points 1–2). Polarity reversal and increase in speed of the hair-bundle movement coincided with the point of the force-displacement relation where the local slope equaled K_{SP} (point 2). A fast recoil of 9.4-nm magnitude was in turn produced (points 2–3), corresponding to a massive reclosure of 65% of the transduction channels. As adaptation proceeded, the system's dynamic operating point left the compliant region of the force-displacement (point 3). Conversely, the hair bundle now moved in the positive direction, slowly reaching a steady-state position in the presence of the constant external force (points 3–4). This positive phase of movement was associated with a component of channel reclosure of similar time course. Note the incomplete character of adaptation. $\lambda = 0.1 \mu\text{N s m}^{-1}$, $\lambda_a = 30 \mu\text{N s m}^{-1}$, $K_{GS} = 1000 \mu\text{N m}^{-1}$, $K_{SP} = 760 \mu\text{N m}^{-1}$, $K_{ES} = 250 \mu\text{N m}^{-1}$, $K_F = 560 \mu\text{N m}^{-1}$, $N = 50$, $D = 37.1 \text{ nm}$, $S = 3.8$, and $F_{\max} = 49 \text{ pN}$. (B) Spontaneous oscillations. The force-displacement relation was here endowed with an unstable region of negative stiffness centered near the operating point. The system displayed spontaneous oscillations of the bundle's position at a frequency of 27 Hz and with a RMS magnitude of 15.8 nm. The fast components of bundle motion, during which the adaptation motor remained almost stationary, were associated with horizontal jumps across the unstable region of the force-displacement relation and abrupt changes of the channels' open probability (points 1–2 and 3–4). The slow components of bundle motion amounted to adaptive movements along the stable branches of the relation (points 2–3) and were produced by a saw-tooth oscillation of the adaptation motor. $\lambda = 0.28 \mu\text{N s m}^{-1}$, $\lambda_a = 10 \mu\text{N s m}^{-1}$, $K_{GS} = 750 \mu\text{N m}^{-1}$, $K_{SP} = 600 \mu\text{N m}^{-1}$, $K_{ES} = 0 \mu\text{N m}^{-1}$, $K_F = 400 \mu\text{N m}^{-1}$, $N = 50$, $D = 60.9 \text{ nm}$, $S = 0.85$, and $F_{\max} = 56 \text{ pN}$. (C) Negative twitch. The force-displacement relation contained here a negative-stiffness region that was centered at a position of –16 nm with respect to the operating point. The system was stable but a negatively directed force step of –30 pN elicited a twitch of 20-nm magnitude and 25-ms duration that qualitatively resembled one-half cycle of the oscillation shown in panel B (points 1–3). The recoil (points 2–3) was associated with a fast jump of the hair bundle across the unstable region of negative stiffness and a massive opening of the transduction channels. Similarly to the positive twitch shown in panel A, this complex, triphasic hair-bundle movement was associated with a monotonic movement of the adaptation motor and the occurrence of a recoil did not require the presence of a negative-stiffness region in the force-displacement relation. $\lambda = 0.28 \mu\text{N s m}^{-1}$, $\lambda_a = 10 \mu\text{N s m}^{-1}$, $K_{GS} = 750 \mu\text{N m}^{-1}$, $K_{SP} = 760 \mu\text{N m}^{-1}$, $K_{ES} = 250 \mu\text{N m}^{-1}$, $K_F = 560 \mu\text{N m}^{-1}$, $N = 50$, $D = 45 \text{ nm}$, $S = 0.3$, and $F_{\max} = 63 \text{ pN}$.

where $\bar{K}_{GS} = K_{GS}(1 - (ZDP_o(1 - P_o))/(k_B T))$ is an effective gating-spring stiffness that accounts for the effect of channel gating (21) on the stiffness K_{GS} of the gating springs, and that depends the open probability P_o of the transduction channels, on the gating force Z , and on the gating swing D (see Table 1). We denote K_{SP} the combined stiffness of stereociliary pivots and stimulus fiber. In the simple case for which the slope $\bar{K}_{GS} + K_{SP}$ of the force-displacement relation is positive for all positions X , a positive adaptive movement δX_a of the motor can thus evoke a negative deflection δX of the hair bundle provided that $\bar{K}_{GS} < 0$ and in turn that:

$$P_o(1 - P_o) > \frac{k_B T}{ZD}. \quad (16)$$

If the open probability of the transduction channels is such that $P_o \cong 0$ or 1, this condition is not satisfied and movements of the adaptation motor and the hair bundle must be in the same direction. If the mechanical effect of channel gating is strong enough that the energy $ZD > 4 k_B T$, however, the hair bundle can move in the direction opposite that of the motor's movement provided that $P_o \cong 0.5$. With such strong gating compliance, there exists a region in the intrinsic force-displacement curve of the hair bundle where the local slope is smaller than the stiffness K_{SP} of the pivots. In this case, an adaptive shift of the force-displacement relation in one direction produces a hair-bundle movement with a directionality that depends on the bundle's operating point within its force-displacement relation (Fig. 2 A). How can the triphasic

hair-bundle movement that describes the twitch be produced in response to positive force steps? If the stimulus initially opens most of the transduction channels, $\bar{K}_{GS} > 0$. The adaptive movement $\delta X_a > 0$ toward the base of the stereocilia of the adaptation motor initially evokes modest reclosure of the transduction channels and simply relaxes gating-spring tension. As a result, the hair-bundle produces an adaptive movement $\delta X > 0$ in the direction of the applied force. However, as P_o approaches one-half, a movement of the motor evokes significant channel reclosure, in turn producing large gating forces in opposition to the external stimulus. If $\bar{K}_{GS} < 0$, this channel gating is strong enough to produce a recoil. The recoil is associated with an increase in gating-spring tension T_{GS} , because $(\partial T_{GS}/\partial X_a)|_X = -\bar{K}_{GS} > 0$. If channels reclose so much that P_o becomes small, \bar{K}_{GS} changes sign again and, correspondingly, the hair bundle reverses the directionality of its adaptive movement. As seen experimentally by others (8,17), the twitch was associated in our numerical calculations with a monotonic adaptive decline of the normalized transduction current that was composed of two kinetic components (Fig. 2 A). Within the framework of our theoretical description, the open probability of the transduction channels is a function of the relative position $X-X_a$ (Eq. 5). In the simple case for which the bundle's position X is clamped and a small step displacement δX is imposed, Eq. 4 indicates that the time course of the adaptive shift δX_a can be described by a single exponential with the characteristic timescale

$$\tau_a = \frac{\lambda_a}{K_{GS} \left(1 - \frac{D}{\delta} \left(1 - S \frac{F_{\max}}{K_{GS} D} \right) P_o (1 - P_o) \right) + K_{ES}}, \quad (17)$$

in which $\delta = k_B T/Z$, K_{ES} is the apparent stiffness of springs that limit the extent of adaptation, λ_a is the slope the force-velocity relation of the adaptation motors, and F_{\max} is the maximal force that these motors can produce. Adaptation kinetics thus depends on the open probability P_o at steady state and on the strength S of Ca^{2+} feedback (Eq. 10). For an operating point in the linear part of the force-displacement relation, where P_o is either near 1 or 0, adaptation is slow: $\tau_a \cong \lambda_a / (K_{GS} + K_{ES}) = 24$ ms for the parameters of Fig. 2 A. In the nonlinear region of the force-displacement region with $P_o \cong 0.5$, adaptation can be fast if

$$S > K_{GS} D / F_{\max}. \quad (18)$$

In this case, Ca^{2+} feedback effectively stiffens the gating springs and, with the same parameters, adaptation is now characterized by $\tau_a = 3.6$ ms. If the hair bundle is stimulated by a force step, the hair-bundle position X varies and thus contributes to adaptation. In the situation depicted in Fig. 2 A, the time course of the adaptive current decline could be fitted by a double exponential, providing two kinetic components of adaptation (19) that were characterized by the time constants $\tau_{\text{fast}} = 0.6$ ms and $\tau_{\text{slow}} = 7.1$ ms. We noticed that adaptation was significantly faster when the bundle position was not clamped and active hair-bundle movements were in

turn allowed to contribute. Spontaneous oscillations required a region of negative stiffness in the force-displacement relation and an operating point located within this unstable region (Fig. 2 B). In this case, a saw-tooth oscillation of the motor's position resulted in a relaxation oscillation of the hair-bundle position and, correspondingly, of the transduction current (12,41). Finally, with a nonlinear force-displacement region centered at a negative displacement with respect to the operating point, the system was stable, displayed slow twitches when stimulated in the negative direction (Fig. 2 C), but relaxed monotonically toward a steady-state position when stimulated in the opposite direction (not shown). As for twitches elicited by positively directed stimuli (Fig. 2 A), the position of the adaptation motor as well as the normalized transduction current relaxed monotonically toward a steady state.

Ca^{2+} effects on hair-bundle mechanics

By using Ca^{2+} iontophoresis to increase the local Ca^{2+} concentration in the vicinity of a hair bundle, we were able to affect the waveform of active hair-bundle movements and, for large enough iontophoretic currents, to evoke transitions between the three classes of bundle motility. Spontaneous hair-bundle oscillations were most commonly observed under two-compartment ionic conditions with 250 μM Ca^{2+} in the artificial endolymph that bathed the hair bundles. For sufficiently large iontophoretic currents, oscillatory hair bundles could become quiescent but would display a twitch in response to positive stimulation. In the example of Fig. 3 A, the recoil was rather blunt at moderate currents, spreading over as much as ~ 80 ms and resembling one-half cycle of a spontaneous oscillation from the same cell. The twitch rapidly sharpened with the concomitant increase of the iontophoretic current, lasting only ~ 4 ms for large currents (Fig. 3 B). There, the hair-bundle movement resembled the fast twitches that have been reported for hair cells totally immersed in standard saline, in which the Ca^{2+} concentration of 4 mM is close to that achieved here with iontophoresis. Faster twitches resulted both from shorter rise times to the local maximum and quicker recoils (not shown). Calcium also affected the magnitude of the negatively directed movement, which decreased linearly by $\sim 50\%$ over the whole range of iontophoretic currents (Fig. 3 C). However, most of the effect of Ca^{2+} on twitch duration occurred within the first 20 nA of iontophoretic current, for which the calcium concentration near the hair bundle increased from 250 μM to ~ 1 mM, whereas the magnitude of the recoil remained roughly constant in that range. When the Ca^{2+} -feedback strength S was increased within a range that spanned one order of magnitude, simulations recapitulated the Ca^{2+} effects on the twitch duration and magnitude (Fig. 3, D–F).

Even under favorable ionic circumstances for the observation of spontaneous oscillations, hair bundles sometimes did not oscillate. However, some of these hair bundles could display a twitch in response to negatively directed stimuli

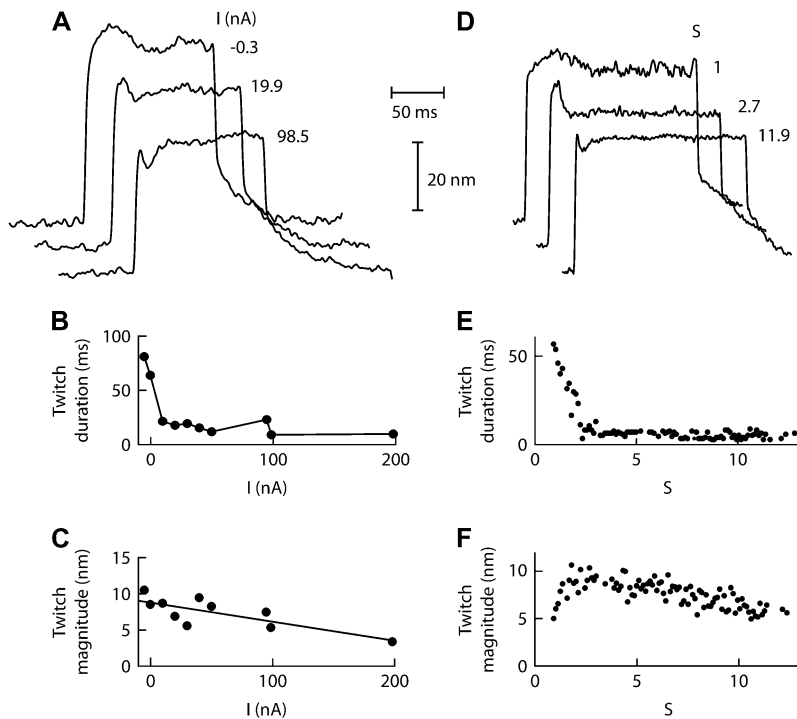


FIGURE 3 Effects of Ca^{2+} iontophoresis on twitch. (A) This hair bundle displayed spontaneous oscillations (16 Hz; RMS magnitude of 19 nm) under control conditions with $250 \mu\text{M}$ Ca^{2+} in the artificial endolymph. A +100-nm displacement of the stimulus fiber's base elicited a twitch (average of 10 presentations) that became sharper and smaller when the iontophoretic current I flowing through an electrode filled with CaCl_2 increased from -0.3 to $+98.5$ nA. A holding current of -10 nA was applied to the iontophoretic electrode that was positioned at $3.7 \mu\text{m}$ from the hair bundle's top. The fiber had a stiffness of $K_F = 227 \mu\text{N m}^{-1}$. (B) The twitch duration, measured as the time interval between the local minimum and the point of same position in the initial rising phase of motion, decreased from 80 ms for moderate currents to 4 ms for large iontophoretic currents. Increasing the iontophoretic current from -5 to 200 nA mediated a local increase of the Ca^{2+} concentration in the vicinity of the transduction channels by about one order of magnitude: with $[\text{Ca}^{2+}] = 250 \mu\text{M}$ at rest, we estimated (Eq. 12) that this concentration fell within the range of $0.4\text{--}7$ mM. (C) The magnitude of the twitch, measured as the displacement between the peak and the local minimum, decreased almost linearly from ~ 10 to ~ 5 nm over the whole range of iontophoretic currents. (D–F) By increasing the Ca^{2+} -feedback strength S from 0.8 to 12, stochastic simulations mimicked the effects of Ca^{2+} on twitch shape (D), duration (E), and magnitude (F). $\lambda = 0.28 \mu\text{N s m}^{-1}$, $\lambda_a = 50 \mu\text{N s m}^{-1}$, $K_{GS} = 800 \mu\text{N m}^{-1}$, $K_{SP} = 540 \mu\text{N m}^{-1}$, $K_{ES} = 1000 \mu\text{N m}^{-1}$, $K_F = 340 \mu\text{N m}^{-1}$, $N = 50$, $D = 40$ nm, and $F_{\text{max}} = 49$ pN.

(Fig. 1 C) or an oscillatory instability when the calcium concentration was sufficiently raised in their proximity (Fig. 4 A). This behavior was associated with a force-displacement relation that showed a nonlinear region of negative slope positioned, before Ca^{2+} iontophoresis was applied, negatively with respect to the operating point (Fig. 4 B). According to our classification of active hair-bundle movements (Fig. 1), the observations shown in Fig. 4 suggest that, in response to an increase of the extracellular calcium concentration, the force-displacement relation shifted positively until the operating point was situated within an unstable region of negative stiffness. As shown in Fig. 5 A for a different cell, we could indeed demonstrate positive shifts of force-displacement relations in response to Ca^{2+} pulses. In this instance, the nonlinear regions of the force-displacement curves were each centered at a point whose abscissa \bar{X}_0 increased linearly with the iontophoretic current (Fig. 5 B). Conversely, we also observed negatively directed shifts of a bundle's force-displacement relation in response to iontophoretic pulses of a Ca^{2+} chelator (not shown). Although a force-displacement relation often appeared to deform as it shifted in response to calcium pulses (Fig. 5 A), the repeatability of force-displacement measurements, especially in its nonlinear region, was rarely precise enough to qualify these deformations for analysis. For one exceptional cell, however, it was possible to demonstrate that Ca^{2+} iontophoresis of large magnitude could affect the shape of

the force-displacement relation (Supplementary Fig. 1, Supplementary Material).

Ca^{2+} -evoked hair-bundle movements

On the basis of Ca^{2+} -evoked shifts of a bundle's force-displacement curve (Fig. 5 A), one can qualitatively anticipate Ca^{2+} -evoked movements of a free or weakly loaded hair bundle (17). Hair-bundle movements have already been reported in response to depolarization of the hair cell's transmembrane potential, a stimulus thought to decrease the driving force for Ca^{2+} entry into the cell through open transduction channels and thus the intracellular Ca^{2+} concentration near the channels' pores (17,22,33,42). In our preparation, we used iontophoresis of Ca^{2+} ions or of a Ca^{2+} chelator provided by either ATP or triphosphate to affect the local extracellular Ca^{2+} concentration near a hair bundle. In each instance, hair bundles responded to iontophoretic pulses by displaying movements, which, for a given type of iontophoresis, could be of either directionality and even be nonmonotonic (Fig. 6). In particular, half of the hair bundles ($n = 14$) responded to an iontophoretic pulse of ATP or triphosphate by a net displacement in the negative direction, whereas the other half moved in the opposite direction. Applying a positive offset of $\sim 1 \mu\text{m}$ to the resting hair-bundle position lowered the fraction of negatively moving bundles to 11% ($n = 18$). This suggests that, similarly to previous observations with hair bundles from

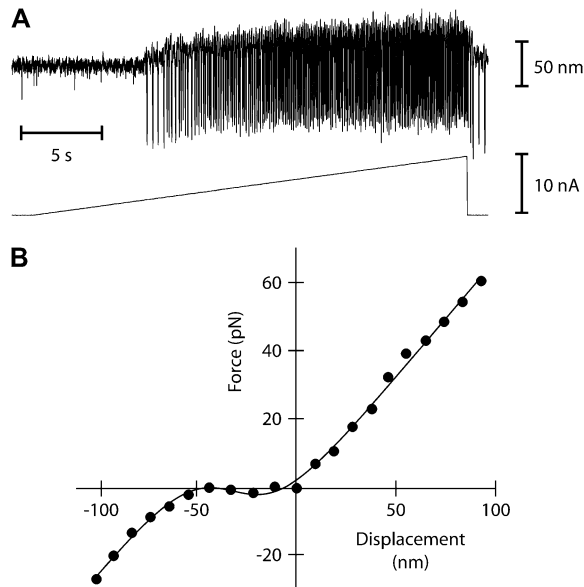


FIGURE 4 From quiescence to spontaneous oscillations with Ca^{2+} iontophoresis. (A) This free-standing hair bundle was quiescent at rest but became oscillatory when Ca^{2+} iontophoresis was used to increase the Ca^{2+} concentration in its vicinity (*ramp* shown at the *bottom*; iontophoretic electrode at $\sim 4 \mu\text{m}$ from the bundle's top). Oscillations appeared abruptly. Although the oscillation frequency almost tripled from ~ 4 to ~ 11 Hz, the peak-to-peak magnitude of the negatively directed spikes remained roughly constant at ~ 100 nm. (B) Under control conditions, the force-displacement relation of the same hair bundle displayed a negative-stiffness region centered at a position of -32 nm with respect to the operating point. A fit with Eq. 1 (*line*) yielded $K_{\infty} = 700 \mu\text{N m}^{-1}$, $N = 159$, and $Z = 0.29$ pN.

the turtle's cochlea (22), the directionality of the movement evoked by a decrease of the extracellular calcium concentration could be reversed by application of a positive offset. Polarity reversals could indeed be observed in response to ATP ($n = 5$ cells), or Ca^{2+} pulses ($n = 4$ cells); one cell could reverse the directionality of its response to both ATP and Ca^{2+} iontophoresis. In the example shown in Fig. 7, the hair bundle displayed a slow negatively directed movement in response to an ATP pulse when delivered with the bundle at its resting position, but the ATP-evoked movement reversed its polarity (Fig. 7, A and B) and increased its speed (Fig. 7 C) when a positive bias larger than $+250$ nm was applied. Simulations qualitatively recapitulated the polarity reversal and change in kinetics of ATP-evoked movements in the presence of a static bias (Fig. 7 D). This can be explained as follows. With the parameters of Fig. 7 D and no offset applied, the channels' open probability $P_o = 11\%$ was not high enough to satisfy the condition expressed by Eq. 16. Under this circumstance, the mechanical effects of adaptive channel gating (here opening) are negligible: the climbing motion of the adaptation motor in response to a decrease in Ca^{2+} , described here by a reduction of Ca^{2+} -feedback strength S , produced an increase of gating-spring tension and thus a negatively directed movement of the hair bundle. Because

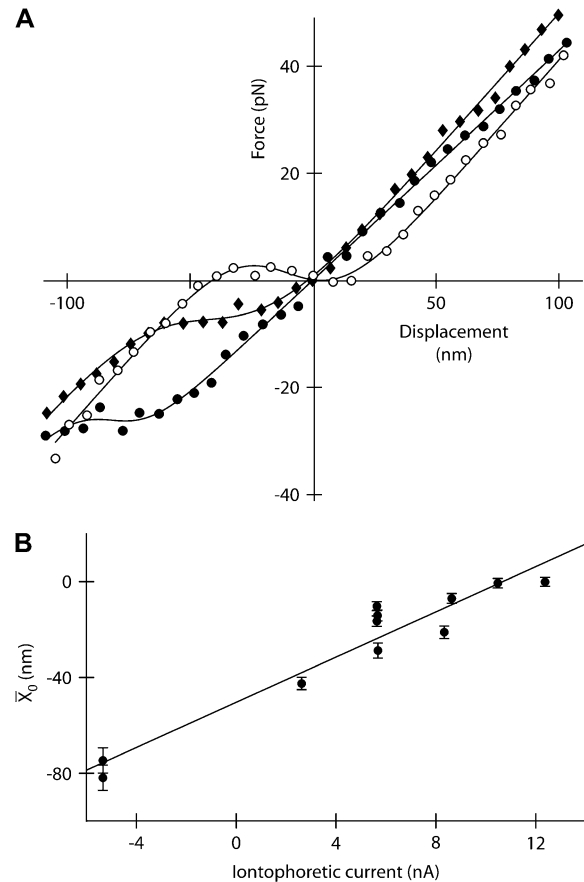


FIGURE 5 Shifts of the force-displacement curve evoked by Ca^{2+} iontophoresis. (A) Measurement of the force-displacement relation for increasing iontophoretic currents (\bullet , -5 nA, holding current; \blacklozenge , $+3$ nA; \circ , $+6$ nA) revealed a positively directed shift. Although the hair bundle was stable under control conditions (\bullet), the bundle's operating point belonged to an unstable region of negative stiffness of the force-displacement relation for an iontophoretic current of $+6$ nA (\circ). Under such circumstances, the hair bundle oscillated spontaneously (not shown). (B) A fit of each force-displacement relations with Eq. 1 allowed the measurement of the deflection \bar{X}_0 for which half of the transduction channels would be open (Eq. 2) as a function of the iontophoretic current I . This relation was well described by a straight line of equation $\bar{X}_0 = 4.72 \times I - 50.4$, in which \bar{X}_0 is in units of nanometers and I of nanoamperes. For each iontophoretic current, hair-bundle deflections were measured with respect to the steady-state position that the hair bundle assumed when no external force was applied; this position depended on the value of the applied iontophoretic current. The iontophoretic pipette was positioned at a distance of $2.5 \mu\text{m}$ from the bundle's top.

adaptation is incomplete, a static offset of $+439$ nm resulted in a significant opening of the transduction channels to $P_o = 32\%$. At this operating point, adaptive gating forces are large enough (Eq. 16) that climbing of the adaptation motor evoked a decrease of gating-spring tension and thus a positively directed movement of the hair bundle. In addition, Ca^{2+} entering the hair cell through open transduction channels effectively stiffens the gating springs (Eq. 18 is fulfilled) resulting in an acceleration of adaptation. Under control conditions, this

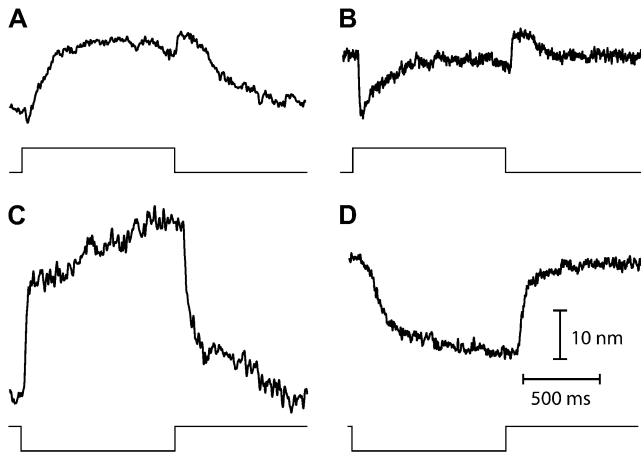


FIGURE 6 Hair-bundle movements evoked by iontophoretic changes of extracellular Ca^{2+} . (A) In response to an iontophoretic pulse of Ca^{2+} , this hair bundle displayed a slow movement in the positive direction, attaining a steady-state position of +13 nm in ~250 ms. (B) Although the stimulus was the same as in panel A, another hair bundle instead displayed a biphasic movement. The bundle first moved rapidly in the negative direction, reaching a local minimum at -12 nm in 23 ms, before slowly progressing in the opposite direction. At steady state, the positive component of motion had almost cancelled the initial negative movement, nearly resulting in no net deflection. (C) This hair bundle was subjected to an iontophoretic pulse of triphosphate, a compound that chelates Ca^{2+} ions. The stimulus evoked a rapid positive movement of 25 nm, followed by a slower drift in the same direction. (D) In contrast, another hair bundle responded to a similar stimulus by moving in the negative direction, reaching a position of -20 nm at the end of the iontophoretic pulse. This negatively directed movement was comparatively slower than the movement of opposite polarity that is shown in panel C. The stimulus was here provided by the iontophoretic release of ATP. The time course of the stimulus is shown as a thin line at the bottom of each record of hair-bundle position. In all cases, the iontophoretic current pulse had an absolute magnitude of 50 nA and the iontophoretic electrode was positioned at a distance of $\sim 3 \mu\text{m}$ from the bundle's top. According to those values and using Eq. 12, the approximate Ca^{2+} concentration that were reached in panels A and B at steady state was $\sim 1.25 \text{ mM}$. When no iontophoretic pipette was present, the hair bundles were immersed in artificial endolymph containing a Ca^{2+} concentration of $250 \mu\text{M}$.

effect is weak, because the channels' open probability remains relatively low, from 11 to only 22%. In the presence of the aforementioned offset, a reduction of S produces massive adaptive opening of the transduction channels from $P_o = 32\%$ to $P_o = 73\%$. There, Ca^{2+} changes have large effects, resulting in a significant acceleration of the bundle's adaptive movement. Note that the polarity of Ca^{2+} -evoked active movement could be reversed by increasing the open probability of the transduction channels by only a few percents. With the parameters of Fig. 7 D but with $F_{\text{max}} = 780 \text{ pN}$ and $P_o = 15\%$, the active movement displays an amplitude of -6 nm. With $F_{\text{max}} = 1020 \text{ pN}$ and $P_o = 23\%$, a movement of +5 nm is observed (not shown). That the system's response to external stimulation could qualitatively change for weak changes of the system's characteristics might explain why different hair bundles displayed movements in opposite directions despite similar experimental conditions (Figs. 1, B and C, and 6).

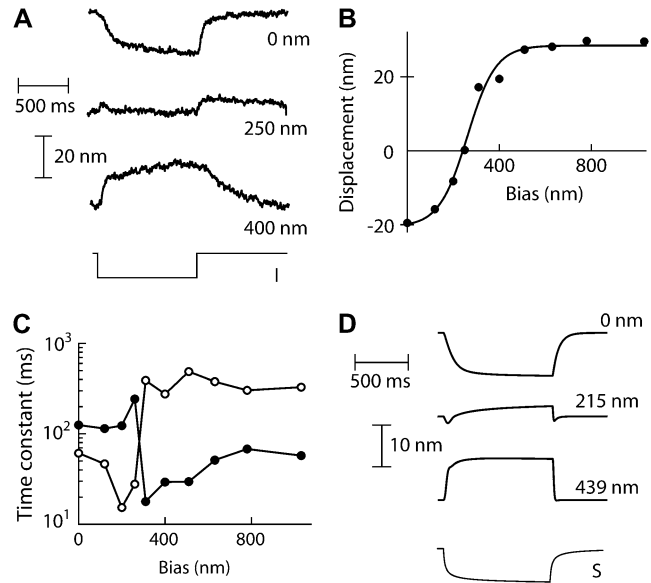


FIGURE 7 Effects of a position bias on hair-bundle movements evoked by a Ca^{2+} chelator. (A) When delivered at the bundle's resting position, an iontophoretic current pulse to $I = -50 \text{ nA}$ through an ATP-containing electrode evoked a slow movement of the hair bundle in the negative direction. After a positive bias of 250 nm had been applied at the bundle's top, the same stimulus produced a small biphasic motion with no significant net deflection at steady state. In the presence of larger biases, here of +400 nm, the ATP-evoked movement displayed faster kinetics and opposite directionality than those measured with no offset. The hair bundle was immersed in artificial endolymph with $250 \mu\text{M}$ Ca^{2+} . In each case, the holding current was +1 nA and the electrode was positioned at $\sim 3 \mu\text{m}$ from the bundle's top. The command to the current generator is represented at the bottom as a thin line. (B) The ATP-evoked displacement of the hair bundle, averaged in the last 10 ms of the iontophoretic pulse, is plotted as a function of the bias. (C) The movements at the onset (●) and the offset (○) of the iontophoretic pulse were each fitted with a single exponential function of time. The corresponding time constants are here plotted as a function of the bias applied at the bundle's top. These plots reveal an abrupt 10-fold change in kinetics at a bias position of +250 nm. (D) Simulations. A step decrease of the Ca^{2+} -feedback strength S by 1.2 produced a movement whose polarity and kinetics depended on the magnitude of a positive bias indicated at the right of each plot. The overall behavior mimics that shown in panel A. The time course of S accounts for diffusion of Ca^{2+} from a point source located $3 \mu\text{m}$ from the system. $\lambda = 1 \mu\text{N s m}^{-1}$, $\lambda_a = 50 \mu\text{N s m}^{-1}$, $K_{\text{GS}} = 750 \mu\text{N m}^{-1}$, $K_{\text{SP}} = 200 \mu\text{N m}^{-1}$, $K_{\text{ES}} = 100 \mu\text{N m}^{-1}$, $K_{\text{F}} = 0 \mu\text{N m}^{-1}$, $N = 100$, $D = 51 \text{ nm}$, $S = 2$, and $F_{\text{max}} = 100 \text{ pN}$.

Active hair-bundle motility in other species

In the cochlea of the turtle, twitches of various shapes have been observed in response to positive step displacements of a stimulus fiber's base (17). Numerical solutions of our model qualitatively reproduced these features (Fig. 8). Mammalian hair bundles from outer hair cells of the rat cochlea can also show complex dynamical behaviors that might be produced by an active process (4). In contrast to hair cells from the bullfrog's sacculus or the turtle's cochlea, no spontaneous oscillations or twitch have yet been observed in this preparation; the hair-bundle responses to step stimuli are monotonic. The

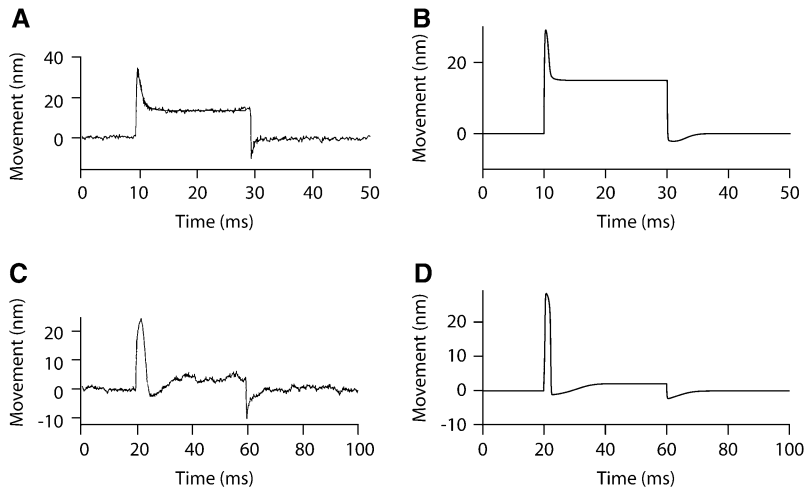


FIGURE 8 Twitches in the turtle cochlea. (A) Hair-bundle movement that was measured in the turtle's cochlea in response to a force step of 37 pN. (B) A similar movement could be obtained in simulations in response to a force step of +40 pN. $\lambda = 0.1 \mu\text{N s m}^{-1}$, $\lambda_a = 10 \mu\text{N s m}^{-1}$, $K_{GS} = 0.4 \text{ mN m}^{-1}$, $K_{SP} = 2 \text{ mN m}^{-1}$, $K_{ES} = 2 \text{ mN m}^{-1}$, $K_F = 0.4 \text{ mN m}^{-1}$, $N = 120$, $D = 150 \text{ nm}$, $S = 3$, and $F_{\text{max}} = 120 \text{ pN}$. (C) Experimental response of another hair bundle to the same stimulus as in panel A. The recoil is here so large that the bundle position overshoots its resting level. (D) A similar movement as that shown in panel C could be simulated if the hair displayed a region of negative stiffness in its intrinsic force-displacement relation (not shown) with a force step of +3 pN. $\lambda = 0.1 \mu\text{N s m}^{-1}$, $\lambda_a = 40 \mu\text{N s m}^{-1}$, $K_{GS} = 0.4 \text{ mN m}^{-1}$, $K_{SP} = 1.5 \text{ mN m}^{-1}$, $K_{ES} = 0 \mu\text{N m}^{-1}$, $K_F = 0.4 \text{ mN m}^{-1}$, $N = 100$, $D = 160 \text{ nm}$, $S = 3$, and $F_{\text{max}} = 90 \text{ pN}$. (A and C from Ricci et al. (17), reprinted with permission.)

steady-state displacement at the tip of a flexible fiber attached to a hair bundle, however, can be larger than that imposed at the fiber's base, which has been interpreted as a signature of active force production by the hair bundle. When measured shortly after the onset of the step stimuli, the force-displacement relation is everywhere of positive slope but displays a compliant region over a displacement range that spans that for channel gating. Allowing more time for adaptation to develop, however, has two consequences. First, the nonlinear region in the force-displacement relation becomes increasingly more compliant, and can even show negative slope at long times. Second, this nonlinear region progressively spreads over a range of displacements that can span several hundreds of nanometers. These observations could be interpreted within the framework of our model with an appropriate choice of parameters (Fig. 9). At steady state, the slope of the force-displacement relation can be calculated from Eqs. 3 and 4 and is given by

$$\left. \frac{dF}{dX} \right|_{\text{stat}} = \frac{1}{1 + \bar{K}_{GS}/K_{ES}} K_{GS} \left(1 - \frac{D}{\delta} P_o (1 - P_o) \right) + K_{SP}. \quad (19)$$

Here,

$$\bar{K}_{GS} = K_{GS} \left(1 - \frac{D}{\delta} \left(1 - \frac{SF_{\text{max}}}{K_{GS}D} \right) P_o (1 - P_o) \right) \quad (20)$$

defines an effective gating-spring stiffness that accounts for the effects of channel gating and Ca^{2+} feedback. If adaptation were complete ($K_{ES} = 0$), the force-displacement relation at steady state would be linear with a constant stiffness K_{SP} . With incomplete adaptation ($K_{ES} \neq 0$), however, Eq. 19 corresponds to a nonlinear force-displacement relation with a stiffness that depends on the open probability P_o . For large displacements, where P_o is zero or one, the stiffness assumes a maximal value of $(dF/dX)|_{\text{stat}} = (K_{GS} K_{ES}) / (K_{ES} + K_{GS}) + K_{SP}$. At the displacement for which $P_o = 0.5$, the stiffness is

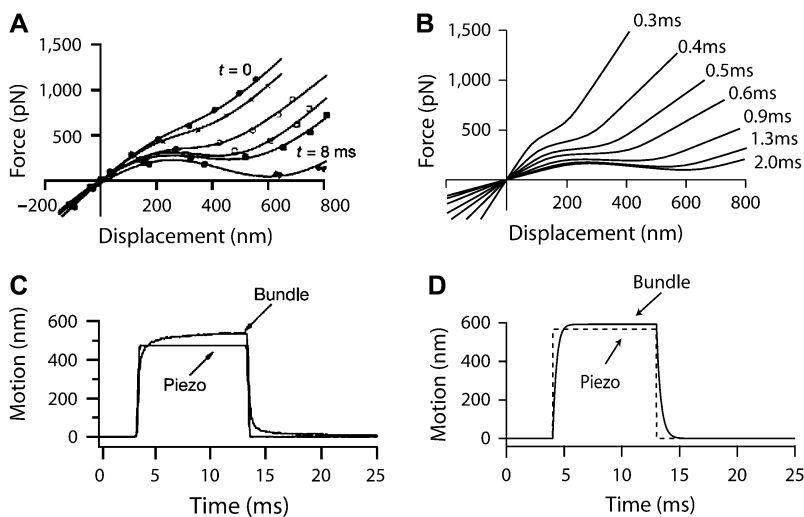


FIGURE 9 Active movements in the rat cochlea. (A) Force-displacement relations that were measured in the rat cochlea at successive times after the transduction current had reached its peak in response to step displacement of the stimulus fiber's base: $t = 0, 0.07, 0.27, 0.47, 0.67, 3.9,$ and 8 ms . (B) Simulated force-displacement relations with the same procedure as in panel A at times reported to the left of each plot. $\lambda = 1 \mu\text{N s m}^{-1}$, $\lambda_a = 0.5 \mu\text{N s m}^{-1}$, $K_{GS} = 8 \text{ mN m}^{-1}$, $K_{SP} = 3.1 \text{ mN m}^{-1}$, $K_{ES} = 750 \mu\text{N m}^{-1}$, $K_F = 3 \text{ mN m}^{-1}$, $N = 150$, $D = 33.1 \text{ nm}$, $S = 4$, and $F_{\text{max}} = 114 \text{ pN}$. (C) In some experiments, the movement of the bundle's tip can exceed that of the fiber's base. (D) The same feature as shown in panel C can be reproduced in simulations with the same parameters as in panel B but $K_{ES} = 1000 \mu\text{N m}^{-1}$, $N = 120$, $D = 45 \text{ nm}$, $S = 6$, and $F_{\text{max}} = 140 \text{ pN}$. (A and C from Kennedy et al. (4), reprinted with permission.)

minimal. With gating compliance strong enough that $K_{GS}(1 - (D/4\delta) + K_{SP}) < 0$, the intrinsic force-displacement relation of the hair bundle displays a region of negative stiffness. In this case, the minimal stiffness given by Eq. 19 is of negative sign, provided that the Ca^{2+} -feedback strength S is large enough to yield $\tilde{K}_{GS} > 0$. In addition, we found that with the parameters of Fig. 9 but with a smaller friction coefficient $\lambda = 0.1 \mu\text{N s}^{-1}$, the hair bundle was stable at rest but that positive offsets could evoke spontaneous hair-bundle oscillations at ~ 5 kHz (Supplementary Fig. 2, Supplementary Material), a frequency near the characteristic frequency of the hair cell whose behavior was described here (4).

DISCUSSION

Directionality and kinetics of adaptive hair-bundle movements

Our theoretical results suggest that a monotonic movement of the adaptation motor can produce deflections of the hair bundle with opposite directionalities (Figs. 2, *A* and *C*, and 7 *D*), depending on how strong the mechanical effects of adaptive channel gating are (Eq. 16). When the transduction channels are either near all open or all closed, a movement of the adaptation motor produces negligible channel gating and thus simply relaxes gating-spring tension. In this case, the directionality of the hair-bundle movement δX is the same as that of the adaptive shift δX_a . Near $P_o = 0.5$, however, a small movement of the adaptation motor can produce a large rearrangement of the channels. This adaptive gating can transiently provide positive feedback on gating-spring tension and in turn produce a movement with a polarity opposite that of the adaptive shift of the motor. This behavior (Eq. 16) happens only in the limit where hair-bundle movements are fast compared to motor movements. If not the case, the motor rapidly adapts to hair-bundle displacement and our calculations, as well as experiments that vary the rise time of the step stimulus (18), indicate that no twitch is produced. This last situation might be relevant to recent experiments in the rat cochlea (4), for which fast adaptation of the transduction current has been measured in response to force steps but neither twitch nor spontaneous oscillations were observed in the bundle's movement (Supplementary Fig. 2, Supplementary Material). In addition, when a hair bundle displays a twitch in response to a force step, the fast kinetics of the recoil contrasts with the slower kinetics of the subsequent movement in the direction of the applied force (Figs. 1 *A* and 2 *A*). In our numerical calculations as well as in published experiments (8,17), these two kinetic components match those found in the associated adaptive decline of the transduction current. This in turn suggests that myosin-based adaptation is enough to describe both fast and slow components of adaptation. Adaptation is fast if the Ca^{2+} -feedback strength S is strong enough that Ca^{2+} entry in the stereocilia effectively stiffens the gating springs and if the

hair bundle operates near $P_o = 0.5$ (Eqs. 17 and 18), but slow otherwise. Because S is proportional to the external Ca^{2+} concentration, the condition for observing fast adaptation is favored by immersing the hair bundles in a high Ca^{2+} medium.

Regulation of active hair-bundle motility

The dynamical behavior of a hair bundle can be modulated by calcium (Figs. 3–5) and by offsets of the bundle's position at steady state (Fig. 7). In our theoretical description, calcium affects only the force F_a that the adaptation motor can produce at stall (Eq. 7) and thus the position X_a that the motor will adopt at steady state (Eq. 4). Our description of hair-bundle mechanics thus accounts for Ca^{2+} -evoked shifts of the force-displacement relation (Fig. 5) and for a change of the bundle's operating point within its force-displacement relation. Assuming that $P_o \cong 1$ (Fig. 5), Eqs. 3, 4, and 6 indicate that $(d\bar{X}_0/dS) \cong (K_{SP})/(K_{GS}K_{SP} + K_{GS}K_{ES} + K_{SP}K_{ES})F_{\max}$. Because the Ca^{2+} -feedback strength S depends linearly on the iontophoretic current (Eq. 13), the measurement $d\bar{X}_0/dI = 4.7 \text{ m/A}^1$ (Fig. 5) provided a means to quantify the Ca^{2+} feedback on the motor force F_a : $dF_a/d[\text{Ca}^{2+}] \approx -5 \mu\text{N M}^{-1}$. At a molecular level, calcium feedback on motor activity could be achieved by several mechanisms. Calcium could affect the probability of an adaptation motor to be bound to actin (30), the stiffness of the actin/myosin cross-bridge (12,20,43), or the size of the power stroke of a single motor (44).

By biasing the bundle's position at steady state, we could reverse the directionality and affect the kinetics of the hair-bundle movements evoked by a pulse of a Ca^{2+} chelator (Fig. 7). We interpret this behavior as a signature of incomplete adaptation: offsets indeed affect the transduction channels' open probability (34) and thus the position of the bundle's operating point within its force-displacement relation at steady state (25). With an operating point that shifts from a steep to a flat region of the force-displacement curve, Ca^{2+} -evoked movements are to change their directionality and kinetics, provided that gating compliance is strong enough (Eq. 16). If the force-displacement relation contains a region of negative stiffness, a quiescent hair bundle may become oscillatory in response to an offset that resettles the operating point within this unstable region (Supplementary Fig. 3, Supplementary Material).

Parameter values in simulations

In the case of the bullfrog's sacculus, most parameter values in the simulations (Table 2) were constrained by measurements from this report and from earlier work by other groups. Fits of force-displacement relations with Eq. 1 provided estimates for K_∞ , N , and Z . Assuming a pivot stiffness $K_{SP} = 200 \mu\text{N m}^{-1}$ (45), we further inferred values for K_{GS} and D . The friction coefficient of both the hair bundle and the

TABLE 2 Parameter values in simulations

Parameter	Fig. 2 A	Fig. 2 B	Fig. 2 C	Fig 3 D–F	Fig 7 D	Fig 8 B	Fig 8 D	Fig 9 B	Fig 9 D
F (pN)	+35	0	–30	25	0, +45, +90	+40	+3	100→3000	1700
K_F (mN m ^{–1})	0.56	0.4	0.56	0.34	0	0.4	0.4	3	3
γ	0.14	0.14	0.14	0.14	0.14	0.06	0.06	0.25	0.25
λ ($\mu\text{N s m}^{-1}$)	0.1	0.28	0.28	0.28	1	0.1	0.1	1	1
λ_a ($\mu\text{N s m}^{-1}$)	30	10	10	50	50	10	40	0.5	0.5
K_{GS} (mN m ^{–1})	1	0.75	0.75	0.8	0.75	0.4	0.4	8	8
k_{GS} (mN m ^{–1})	0.98	0.735	0.735	0.784	0.735	1.11	1.11	0.853	1.067
K_{SP} (mN m ^{–1})	0.76	0.6	0.76	0.54	0.2	2	1.5	3.1	3.1
K_{ES} (mN m ^{–1})	0.25	0	0.25	1	0.1	0	0	0.75	1
K_∞ (mN m ^{–1})	1.2	0.95	0.95	1	0.95	2	1.5	8	8
N	50	50	50	50	100	120	100	150	120
D (nm)	37.1	60.9	45	40	51	150	160	33.1	45
d (nm)	5.3	8.7	6.4	5.7	7.3	9	9.6	8.3	11.3
S	3.8	0.85	0.3	0.8→12	2→0.8	3	3	4	6
F_{\max} (pN)	49	56	63	49	100	120	90	114	140
v_{\max} ($\mu\text{m s}^{-1}$)	0.229	0.784	0.882	0.137	0.280	0.720	0.135	57	70

attached stimulus fiber was in the range $\lambda \cong 0.1\text{--}1 \mu\text{N s m}^{-1}$ (30,46). The maximal motor force F_{\max} and Ca^{2+} -feedback strength S controlled the location of bundle's operating point along the force-displacement curve and thus the open probability of the transduction channels at steady state. In accordance with a previous estimate (30) of the average force that can be generated by ~ 3000 myosin-based motor molecules within a hair bundle (47), F_{\max} was fixed in the range 50–100 pN in most of our simulations. In contrast, S was adjusted within in a relatively broad range of 0.3–12. This parameter varies linearly with the extracellular Ca^{2+} concentration (Eqs. 10 and 11), which spanned more than one order of magnitude in our experiments. For large values of S , a situation that is favored by high extracellular Ca^{2+} , the motors are weak (Eq. 9) and the open probability of the transduction channels is correspondingly low; the converse is true for small values of this parameter. Note that for values of $S > 1$, the simple linear dependence of the active motor force F_a with the Ca^{2+} concentration (Eq. 7) allows F_a to become negative in sign. Although they bear no physical significance, negative motor forces F_a do not qualitatively affect the active hair-bundle movements that are calculated by the model: a more complex model in which we impose $F_a = 0$ when $SP_o > 1$ produces similar movements (not shown). When the incompleteness of adaptation could not be ignored, we adjusted the stiffness K_{ES} of the extent spring to ensure that, in response to a step deflection \bar{X} of the hair bundle, the motor would move from its initial steady-state position by $\bar{X}_a \cong 0.7 - 0.9 \bar{X}$ (20,34). A study of the initial adaptation rate as a function of the magnitude of positive step stimuli (36) provided the estimate $\lambda_a \cong 10\text{--}50 \mu\text{N s m}^{-1}$ for the slope of the motor's force-velocity curve. Note that all parameters are here expressed along the bundle's horizontal axis of maximal mechanosensitivity at the bundle's top. Comparing numerical values of a given parameter between different hair cells is not straightforward. In particular, parameter D is related to the microscopic gating swing d by a

geometrical factor γ that depends on bundle geometry and thus on species: $d = \gamma D$ (48). Similarly, the combined stiffness K_{GS} of the gating springs is related to the intrinsic molecular stiffness k_{GS} of a single gating spring by: $K_{GS} = N \gamma^2 k_{GS}$. Typical values are: $\gamma = 0.14$ for the bullfrog sacculus (24); $\gamma = 0.06$ for the turtle's cochlea (49); $\gamma = 0.25$ for the rat's cochlea at a 0.8 fractional distance from the base (R. Fettiplace, personal communication, 2005). Although large variations of D and K_{GS} might appear necessary to describe different species, the microscopic parameters d and k_{GS} in fact lay within relatively narrow ranges of 5.3–11.3 nm and 0.74–1.1 mN m^{–1}, respectively. These values are in accordance with those previously reported for the bullfrog's sacculus (21,23,25). The molecular origin of the dispersion within these ranges is not established but this work provides evidence that Ca^{2+} might be involved (Supplementary Fig. 1, Supplementary Material). To account for fast adaptation in the rat cochlea (4,50), it was necessary to assume a value $\lambda_a = 0.5 \mu\text{N s m}^{-1}$ that was 20- to 100-fold smaller than those used for the frog and the turtle.

Active movements of mammalian hair bundles

The same physical description that accounts for active hair-bundle movements in the bullfrog's sacculus and the turtle's cochlea can describe the behavior of hair bundles from the rat cochlea (Fig. 9). Adaptation in the rat, with a characteristic timescale as short as $\sim 100 \mu\text{s}$ at a 0.2 fractional distance from the cochlea's apex (50,51), is significantly faster than in the turtle's cochlea or the bullfrog's sacculus. Can myosin-based adaptation be this fast? In our simulations, adaptation kinetics is controlled in part by λ_a (Eq. 4). To account for fast adaptation in the rat cochlea, a value of $\lambda_a = 0.5 \mu\text{N s m}^{-1}$ that was 20- to 100-fold smaller than those used for the other species was required. If the adaptation motor obeyed a linear force-velocity relation, one would in turn anticipate a maximal climbing velocity of $v_{\max} =$

$\gamma F_{\max}/\lambda_a = 55 \mu\text{m s}^{-1}$ when the motor is not subjected to an external force. Here, we used the parameters of Fig. 9 and the geometrical gain of stereociliary shear motion $\gamma = 0.25$ (R. Fettiplace, personal communication, 2005) to express the motor velocity along the longitudinal axis of the stereocilia. This value of v_{\max} is abnormally high when compared to the motor velocities that have been measured in vitro under weak external loads with myosin molecules, in particular with myosin 1c (44,52,53). Under physiological circumstances, however, the adaptation motor operates near stall force. Therefore, the value of λ_a is required to describe the slope of the motor's force-velocity relation near stall only but not necessarily at weaker forces. If the force-velocity relation of the adaptation motor were nonlinear, v_{\max} could thus overestimate the motor's maximal climbing velocity. Non-processive myosin molecules, such as myosin 1c, must work in groups. It was shown on theoretical grounds that the force-velocity relation of a collection of molecular motors can indeed become nonlinear and display a point of inflection of low slope near stall force (54). The small value of λ_a might reflect nonlinear collective effects that allow a relatively slow motor assembly under low load to respond briskly to any small perturbation near stall, thereby mediating adaptation at a sufficient speed to account for the associated hair-bundle movements in the rat cochlea.

Other mechanisms of adaptation

We have shown that the motor that underlies slow adaptation can also produce fast adaptation as the result of strong nonlinear gating compliance and Ca^{2+} feedback (Eqs. 17 and 18). This finding is consistent with the proposal that the fast component of adaptation results from a conformational release of the adaptation motor (20), for such movement would amount to an adaptive shift δX_a . Other groups argued that Ca^{2+} entry stabilizes the closed state of the transduction channels (17,21–23). This mechanism finds support from the force dependence of the twitch elicited by depolarization and repolarization of a hair cell (23). Our description, however, could account for a similar dependence (Supplementary Fig. 4, Supplementary Material). In addition, although fast and slow components of adaptation are often associated with hair-bundle movements of opposite directionalities, myosin-based adaptation can account for this observation (Fig. 2A). This analysis is fostered by the recent finding that myosin-1c mediates both fast and slow adaptation in hair cells from the vestibular systems of the bullfrog and the mouse (20).

Although a hair bundle is very complex, our simple description of its mechanical properties appears to suffice to interpret the salient features of active hair-bundle motility. Only three ingredients are involved: strong gating compliance, myosin-based adaptation, and Ca^{2+} feedback on the motor's activity. Because this description also applies to hair-bundle movements in the cochlea of the turtle and the rat, our results suggests that hair cells from different species

might use a conserved mechanism of active force production by their hair bundles.

SUPPLEMENTARY MATERIAL

To view all of the supplemental files associated with this article, visit www.biophysj.org.

We thank Björn Nadrowski for stimulating discussions.

J.-Y.T. and P.M. were supported by Human Frontier Science Program grant RGP0051/2003 and by European Commission FP6 Integrated Project EUROHEAR, LSHG-CT-2004-512063. J.-Y.T. was supported by Fondation pour la Recherche Médicale grant FDT20050703805.

REFERENCES

- Hudspeth, A. J. 1997. Mechanical amplification of stimuli by hair cells. *Curr. Opin. Neurobiol.* 7:480–486.
- Brownell, W. E., C. R. Bader, D. Bertrand, and Y. de Ribaupierre. 1985. Evoked mechanical responses of isolated cochlear outer hair cells. *Science.* 227:194–196.
- Santos-Sacchi, J. 2003. New tunes from Corti's organ: the outer hair cell boogie rules. *Curr. Opin. Neurobiol.* 13:459–468.
- Kennedy, H. J., A. C. Crawford, and R. Fettiplace. 2005. Force generation by mammalian hair bundles supports a role in cochlear amplification. *Nature.* 433:880–883.
- Chan, D. K., and A. J. Hudspeth. 2005. Ca^{2+} current-driven nonlinear amplification by the mammalian cochlea in vitro. *Nat. Neurosci.* 8:149–155.
- Manley, G. A. 2001. Evidence for an active process and a cochlear amplifier in nonmammals. *J. Neurophysiol.* 86:541–549.
- Crawford, A. C., and R. Fettiplace. 1985. The mechanical properties of ciliary bundles of turtle cochlear hair cells. *J. Physiol.* 364:359–379.
- Howard, J., and A. J. Hudspeth. 1987. Mechanical relaxation of the hair bundle mediates adaptation in mechano-electrical transduction by the bullfrog's saccular hair cell. *Proc. Natl. Acad. Sci. USA.* 84:3064–3068.
- Rusch, A., and U. Thurm. 1990. Spontaneous and electrically induced movements of ampullary kinocilia and stereovilli. *Hear. Res.* 48:247–263.
- Denk, W., R. M. Keolian, and W. W. Webb. 1992. Mechanical response of frog saccular hair bundles to the aminoglycoside block of mechano-electrical transduction. *J. Neurophysiol.* 68:927–932.
- Martin, P., and A. J. Hudspeth. 1999. Active hair-bundle movements can amplify a hair cell's response to oscillatory mechanical stimuli. *Proc. Natl. Acad. Sci. USA.* 96:14306–14311.
- Martin, P., D. Bozovic, Y. Choe, and A. J. Hudspeth. 2003. Spontaneous oscillation by hair bundles of the bullfrog's sacculus. *J. Neurosci.* 23:4533–4548.
- Martin, P., and A. J. Hudspeth. 2001. Compressive nonlinearity in the hair bundle's active response to mechanical stimulation. *Proc. Natl. Acad. Sci. USA.* 98:14386–14391.
- Choe, Y., M. O. Magnasco, and A. J. Hudspeth. 1998. A model for amplification of hair-bundle motion by cyclical binding of Ca^{2+} to mechano-electrical-transduction channels. *Proc. Natl. Acad. Sci. USA.* 95:15321–15326.
- Eguiluz, V. M., M. Ospeck, Y. Choe, A. J. Hudspeth, and M. O. Magnasco. 2000. Essential nonlinearities in hearing. *Phys. Rev. Lett.* 84:5232–5235.
- Camalet, S., T. Duke, F. Jülicher, and J. Prost. 2000. Auditory sensitivity provided by self-tuned critical oscillations of hair cells. *Proc. Natl. Acad. Sci. USA.* 97:3183–3188.
- Ricci, A. J., A. C. Crawford, and R. Fettiplace. 2000. Active hair bundle motion linked to fast transducer adaptation in auditory hair cells. *J. Neurosci.* 20:7131–7142.

18. Benser, M. E., R. E. Marquis, and A. J. Hudspeth. 1996. Rapid, active hair bundle movements in hair cells from the bullfrog's sacculus. *J. Neurosci.* 16:5629–5643.
19. Wu, Y. C., A. J. Ricci, and R. Fettiplace. 1999. Two components of transducer adaptation in auditory hair cells. *J. Neurophysiol.* 82:2171–2181.
20. Stauffer, E. A., J. D. Scarborough, M. Hirono, E. D. Miller, K. Shah, J. A. Mercer, J. R. Holt, and P. G. Gillespie. 2005. Fast adaptation in vestibular hair cells requires myosin-1c activity. *Neuron.* 47:541–553.
21. Howard, J., and A. J. Hudspeth. 1988. Compliance of the hair bundle associated with gating of mechano-electrical transduction channels in the bullfrog's saccular hair cell. *Neuron.* 1:189–199.
22. Ricci, A. J., A. C. Crawford, and R. Fettiplace. 2002. Mechanisms of active hair bundle motion in auditory hair cells. *J. Neurosci.* 22:44–52.
23. Cheung, E. L. M., and D. P. Corey. 2006. Ca^{2+} changes the force sensitivity of the hair-cell transduction channel. *Biophys. J.* 90:124–139.
24. Jacobs, R. A., and A. J. Hudspeth. 1990. Ultrastructural correlates of mechano-electrical transduction in hair cells of the bullfrog's internal ear. *Cold Spring Harb. Symp. Quant. Biol.* 55:547–561.
25. Martin, P., A. D. Mehta, and A. J. Hudspeth. 2000. Negative hair-bundle stiffness betrays a mechanism for mechanical amplification by the hair cell. *Proc. Natl. Acad. Sci. USA.* 97:12026–12031.
26. Wilson, J. E., and A. Chin. 1991. Chelation of divalent cations by ATP, studied by titration calorimetry. *Anal. Biochem.* 193:16–19.
27. Housley, G. D., R. Kanjhan, N. P. Raybould, D. Greenwood, S. G. Salih, L. Jarlebark, L. D. Burton, V. C. Setz, M. B. Cannell, C. Soeller, D. L. Christie, S. Usami, et al. 1999. Expression of the P2X(2) receptor subunit of the ATP-gated ion channel in the cochlea: implications for sound transduction and auditory neurotransmission. *J. Neurosci.* 19:8377–8388.
28. Dulon, D., P. Mollard, and J. M. Aran. 1991. Extracellular ATP elevates cytosolic Ca^{2+} in cochlear inner hair cells. *Neuroreport.* 2:69–72.
29. Aubert, A., C. H. Norris, and P. S. Guth. 1994. Influence of ATP and ATP agonists on the physiology of the isolated semicircular canal of the frog (*Rana pipiens*). *Neuroscience.* 62:963–974.
30. Nadrowski, B., P. Martin, and F. Jülicher. 2004. Active hair-bundle motility harnesses noise to operate near an optimum of mechanosensitivity. *Proc. Natl. Acad. Sci. USA.* 101:12195–12200.
31. Iwasa, K. H., and G. Ehrenstein. 2002. Cooperative interaction as the physical basis of the negative stiffness in hair cell stereocilia. *J. Acoust. Soc. Am.* 111:2208–2212.
32. Kozlov, A. S., T. Risler, and A. J. Hudspeth. 2007. Coherent motion of stereocilia assures the concerted gating of hair-cell transduction channels. *Nat. Neurosci.* 10:87–92.
33. Assad, J. A., and D. P. Corey. 1992. An active motor model for adaptation by vertebrate hair cells. *J. Neurosci.* 12:3291–3309.
34. Shepherd, G., and D. Corey. 1994. The extent of adaptation in bullfrog saccular hair cells. *J. Neurosci.* 14:6217–6229.
35. Frank, J. E., V. Markin, and F. Jaramillo. 2002. Characterization of adaptation motors in saccular hair cells by fluctuation analysis. *Biophys. J.* 83:3188–3201.
36. Hacohen, N., J. A. Assad, W. J. Smith, and D. P. Corey. 1989. Regulation of tension on hair-cell transduction channels: displacement and calcium dependence. *J. Neurosci.* 9:3988–3997.
37. Crawford, A. C., M. G. Evans, and R. Fettiplace. 1991. The actions of calcium on the mechano-electrical transducer current of turtle hair cells. *J. Physiol.* 434:369–398.
38. Corey, D. P., and A. J. Hudspeth. 1983. Analysis of the microphonic potential of the bullfrog's sacculus. *J. Neurosci.* 3:942–961.
39. Lumpkin, E. A., and A. J. Hudspeth. 1998. Regulation of free Ca^{2+} concentration in hair-cell stereocilia. *J. Neurosci.* 18:6300–6318.
40. Berg, H. C. 1993. *Random Walks in Biology*. Princeton University Press, Princeton, NJ.
41. Le Goff, L., D. Bozovic, and A. J. Hudspeth. 2005. Adaptive shift in the domain of negative stiffness during spontaneous oscillation by hair bundles from the internal ear. *Proc. Natl. Acad. Sci. USA.* 102:16996–17001.
42. Assad, J. A., N. Hacohen, and D. P. Corey. 1989. Voltage dependence of adaptation and active bundle movement in bullfrog saccular hair cells. *Proc. Natl. Acad. Sci. USA.* 86:2918–2922.
43. Howard, J., and J. A. Spudich. 1996. Is the lever arm of myosin a molecular elastic element? *Proc. Natl. Acad. Sci. USA.* 93:4462–4464.
44. Batters, C., C. P. Arthur, A. Lin, J. Porter, M. A. Geeves, R. A. Milligan, J. E. Molloy, and L. M. Coluccio. 2004. Myo1c is designed for the adaptation response in the inner ear. *EMBO J.* 23:1433–1440.
45. Marquis, R. E., and A. J. Hudspeth. 1997. Effects of extracellular Ca^{2+} concentration on hair-bundle stiffness and gating-spring integrity in hair cells. *Proc. Natl. Acad. Sci. USA.* 94:11923–11928.
46. Denk, W., W. W. Webb, and A. J. Hudspeth. 1989. Mechanical properties of sensory hair bundles are reflected in their Brownian motion measured with a laser differential interferometer. *Proc. Natl. Acad. Sci. USA.* 86:5371–5375.
47. Gillespie, P. G., M. C. Wagner, and A. J. Hudspeth. 1993. Identification of a 120 kd hair-bundle myosin located near stereociliary tips. *Neuron.* 11:581–594.
48. Markin, V. S., and A. J. Hudspeth. 1995. Gating-spring models of mechano-electrical transduction by hair cells of the internal ear. *Annu. Rev. Biophys. Biomol. Struct.* 24:59–83.
49. Hackney, C. M., R. Fettiplace, and D. N. Furness. 1993. The functional morphology of stereociliary bundles on turtle cochlear hair cells. *Hear. Res.* 69:163–175.
50. Kennedy, H. J., M. G. Evans, A. C. Crawford, and R. Fettiplace. 2003. Fast adaptation of mechano-electrical transducer channels in mammalian cochlear hair cells. *Nat. Neurosci.* 6:832–836.
51. Ricci, A. J., H. J. Kennedy, A. C. Crawford, and R. Fettiplace. 2005. The transduction channel filter in auditory hair cells. *J. Neurosci.* 25:7831–7839.
52. Gillespie, P. G., S. K. Gillespie, J. A. Mercer, K. Shah, and K. M. Shokat. 1999. Engineering of the myosin- β nucleotide-binding pocket to create selective sensitivity to N(6)-modified ADP analogs. *J. Biol. Chem.* 274:31373–31381.
53. Inoue, A., and M. Ikebe. 2003. Characterization of the motor activity of mammalian myosin VIIA. *J. Biol. Chem.* 278:5478–5487.
54. Jülicher, F., A. Ajdari, and J. Prost. 1997. Modeling molecular motors. *Rev. Mod. Phys.* 69:1269–1281.